Correction to Arrays of ZnO/Zn(x)Cd(1−x)Se Nanocables: Band Gap Engineering and Photovoltaic Applications.

ARTICLE *in* NANO LETTERS · APRIL 2012

Impact Factor: 13.59 · DOI: 10.1021/nl301181u · Source: PubMed

NANO LETTERS

LETTER

pubs.acs.org/NanoLett

Arrays of ZnO/$Zn_xCd_{1-x}Se$ Nanocables: Band Gap Engineering and Photovoltaic Applications

Jun Xu,[†,‡] Xia Yang,[†,‡] Hongkang Wang,[†] Xue Chen,[†,‡] Chunyan Luan,[†,‡] Zongxiang Xu,[†] Zhenzhen Lu,[†,‡] V. A. L. Roy,[†] Wenjun Zhang,[†,‡] and Chun-Sing Lee*[,†,‡]

[†]Department of Physics and Materials Science and [‡]Center of Super-Diamond and Advanced Films (COSDAF), City University of Hong Kong, Hong Kong SAR, People's Republic of China

Supporting Information

ABSTRACT: Arrays of ZnO/$Zn_xCd_{1-x}Se$ ($0 \le x \le 1$) core/shell nanocables with shells of tunable compositions have been synthesized on fluorine-doped tin oxide glass substrates via a simple ion-exchange approach. Through the effects of stoichiometry and type II heterojunction, optical absorptions of the nanocable arrays can be controllably tuned to cover almost the entire visible spectrum. Lattice parameters and band gaps of the ternary $Zn_xCd_{1-x}Se$ shells were found to have respectively linear and quadratic relationships with the Zn content (x). These ZnO/$Zn_xCd_{1-x}Se$ nanocable arrays are further demonstrated to be promising photoelectrodes for photoelectrochemical solar cells, giving a maximum power conversion efficiency up to 4.74%.

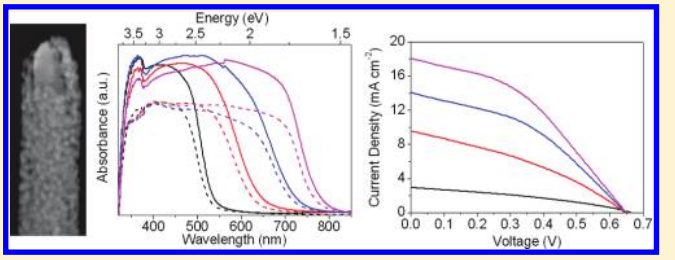

KEYWORDS: ZnSe, CdSe, type II, band gap engineering, Vegard's law, solar cells

Band gap engineering is an important strategy for custom tuning physical properties of semiconductors in optoelectronic devices.[1−3] On comparison with bulk semiconductors, nanostructured materials provide a novel way for band gap modulation through their tunable sizes and shapes due to the quantum confinement effects.[4−6] Band gap tuning of multinary alloyed nanostructures has been achieved via compositional effect, which arises from a strong dependence of electronic energies on the effective exciton mass.[7−10] Furthermore, an additional approach for band gap engineering can also be achieved in core/shell heterostructures. For example, type II core/shell heterostructures have band gaps that form a stepwise energy alignment at the heterojunctions, where both the conduction and the valence bands of the shell are either higher or lower in energy than those of the core. Electrons and holes would preferably transfer across the interface in opposite directions to form an excitonic charge separation state.[11,12] Absorption/emission of photons through separation/recombination between holes confined in one component and electrons confined in the other component occurs across the interface at a lower energy than the band gaps of either of the constituent semiconductors, adding a new dimension of band gap engineering. Therefore, type II core/shell nanostructures with multinary alloyed constituents may give a multidimensional control for band gap engineering to get highly tunable optoelectronic properties.[13−15]

In the past 2 decades, much attention has been put on quantum dot sensitized solar cells (QDSSCs) based on one-dimensional (1D) ZnO and/or TiO_2 nanoarrays, sensitized by various quantum dots (QD)/nanocrystals such as CdS,[16−18] CdSe,[19−22] CdTe,[23,24] $CuInS_2$,[25] and Cu_2O.[26] Power conversion efficiencies of these QDSSCs are typically less than 4%. Their performances are typically limited by problems of aggregation, low QD loading density, and interface problems from organic linker molecules between the QDs and the nanowires.[19,27−29]

Arrays of type II core/shell heterogeneous nanocables are considered as promising photoelectrodes for photovoltaic (PV) applications to solve these problems with additional advantages for light absorption, charge separation, and transportation.[30,31] The staggered type II heterojunctions can extend their absorption profiles to cover wavelengths longer than that defined by the band gap of both the constituting components.[32−34] The core/shell nanocables not only provide large interfacial area for charge separation but also ensure that the carrier separation would take place along the shorter radial instead of the longer axial direction and thus increase the carrier collection efficiency.[35] Furthermore, the vertically aligned 1D structures provide a direct pathway for rapid transport of photogenerated carriers to the collection electrode.[36] The core/shell structure can also provide effective passivation that inhibits nonradiative recombination of percolated electrons in 1D oxide with electrolyte and provides corrosion protection to the oxide cores from electrolyte.[37] Herein, we design and report an ion-exchange route to prepare arrays of type II ZnO/$Zn_xCd_{1-x}Se$ core/shell nanocables with tunable shell composition ($0 \le x \le 1$) and band gaps from 1.62 to 2.33 eV. On the basis of the nanocable arrays, a PV device with a maximum power conversion efficiency of 4.74% has been demonstrated.

Received: June 8, 2011
Revised: August 17, 2011
Published: August 29, 2011

Scheme 1. Schematic Illustration for the Formation Processes of the ZnO/$Zn_xCd_{1-x}Se$ Core/Shell Nanocables

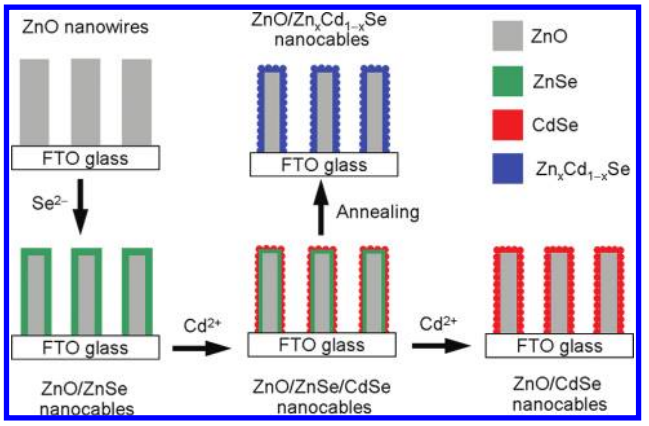

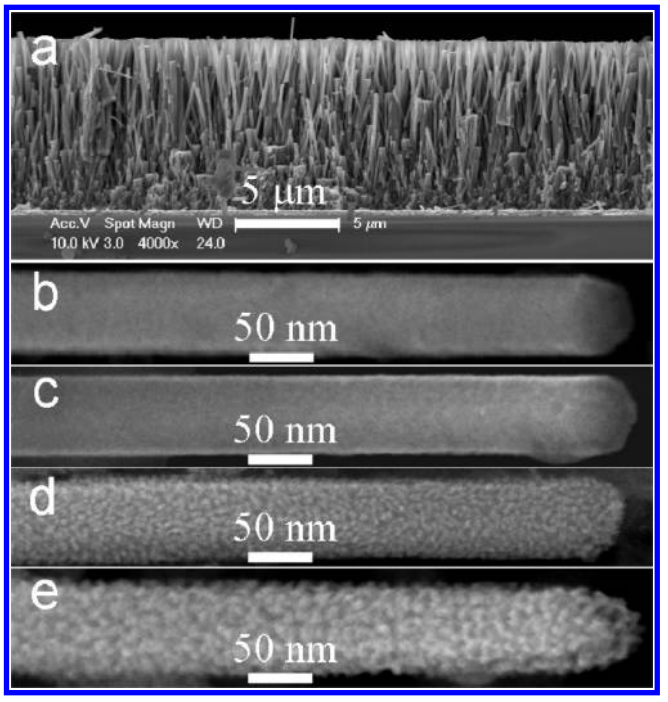

Figure 1. SEM images of (a) a ZnO nanowire array, (b) a ZnO/ZnSe nanocable, (c) a $Zn_{0.7}Cd_{0.3}Se$ nanocable prepared by reacting a ZnO/ZnSe nanocable with Cd^{2+} at 50 °C, (d) a ZnO/$Zn_{0.33}Cd_{0.67}Se$ nanocable prepared by reacting a ZnO/ZnSe nanocable with Cd^{2+} at 90 °C, and (e) a ZnO/CdSe nanocable prepared by reacting a ZnO/ZnSe nanocable with Cd^{2+} at 140 °C.

Strategy for the synthesis of the arrays of ZnO/$Zn_xCd_{1-x}Se$ core/shell nanocables is illustrated in Scheme 1. The solubility product constant (K_{sp}) of ZnO (6.8×10^{-17}) is much larger than those of ZnSe (3.6×10^{-26}) and CdSe (6.31×10^{-36}). This implies that the arrays of ZnO nanowires can be used as sacrificial templates to synthesize more stable ZnSe by anion exchange and further convert into CdSe by cation exchange. In our case, the array of ZnO/ZnSe/CdSe nanocables is prepared by surface selenization of ZnO nanowires with Se^{2-} ions to form ZnO/ZnSe nanocables,[38] and followed with partial conversion of ZnSe to CdSe through ion replacement of Zn^{2+} by Cd^{2+} in the ZnSe

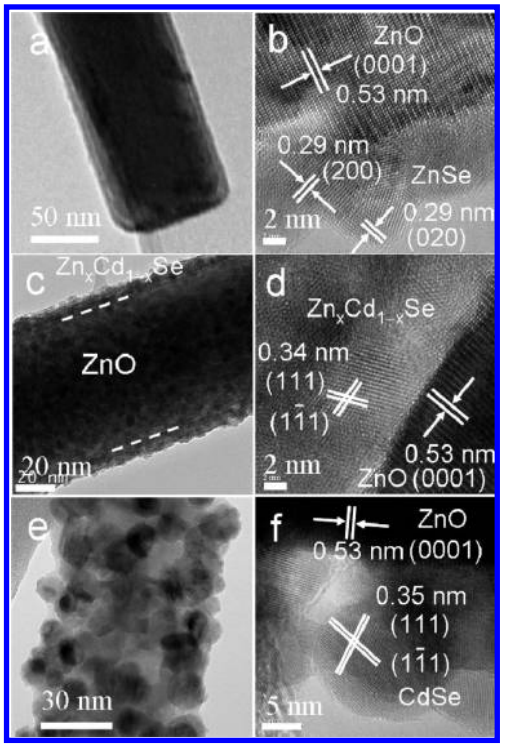

Figure 2. TEM and high-resolution TEM images of (a, b) a ZnO/ZnSe nanocable, (c, d) a ZnO/$Zn_{0.33}Cd_{0.67}Se$ nanocable, and (e, f) a ZnO/CdSe nanocable.

shells. Different ratios of Cd/Zn in the ZnSe/CdSe bilayer shell can be achieved by controlling the reaction temperature of the ZnO/ZnSe nanocables with Cd^{2+} ions. Homogeneous ternary alloyed $Zn_xCd_{1-x}Se$ ($0 \leq x \leq 1$) shells can be obtained by annealing the trilayer ZnO/ZnSe/CdSe nanocables at 400 °C, leading to the formation of corresponding bilayer ZnO/$Zn_xCd_{1-x}Se$ nanocables. The two components ZnSe and CdSe in the trilayer cables differ only in their cations. However, the two components in the ZnO/ZnSe and the ZnO/CdSe core/shell nanocables differ either in their anions or in both the anions and the cations. As group II cations have much smaller sizes and diffuse faster than the group VI anions in the II−VI semiconductors, upon annealing the outer ZnSe/CdSe interface in the trilayer cables can be intermixed to form an alloy easier than the inner ZnO/ZnSe and ZnO/CdSe core/shell interfaces.

Figure 1a shows a typical SEM image of an array of ZnO nanowires with lengths of about 9 μm and diameters of 50−150 nm. Magnified SEM images of the ZnO/$Zn_xCd_{1-x}Se$ nanocables are presented in panels b−e of Figure 1, showing the nanocables have rougher surface with increasing Cd content in the shells. Compositions of the $Zn_xCd_{1-x}Se$ shells, prepared by immersing the ZnO/$Zn_xCd_{1-x}Se$ nanocables in an acetic acid solution to remove the ZnO cores, were measured from their EDX spectra (Figure S1, Supporting Information). A layer of CdSe nanoparticles is uniformly and compactly covered on the surface of ZnO nanowires to form a ZnO/CdSe nanocable as shown in Figure 1e.

The structures of the ZnO/$Zn_xCd_{1-x}Se$ core/shell nanocables are further demonstrated by their TEM and high-resolution TEM images in Figure 2. Figure 2a shows a typical TEM image of a ZnO/ZnSe nanocable. Across the cable, the brightness profile shows a clear variation with a light-contrasted shell of about

dx.doi.org/10.1021/nl201934k |*Nano Lett.* 2011, 11, 4138–4143

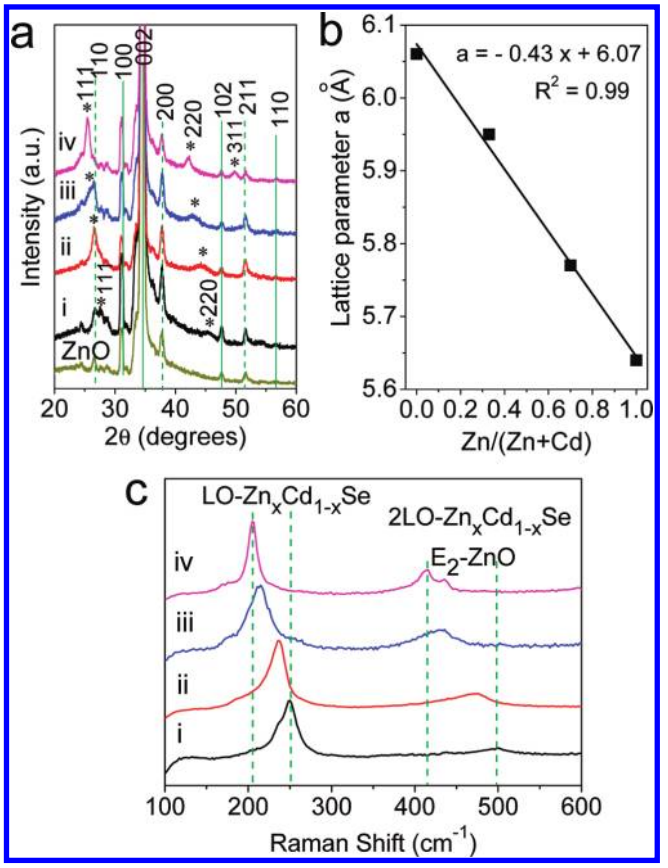

Figure 3. (a) XRD data of the arrays of bare ZnO nanowires and ZnO/$Zn_xCd_{1-x}Se$ ($0 \le x \le 1$) nanocables grown on FTO glass substrates. (b) A linear relationship of the lattice parameter a of the ternary $Zn_xCd_{1-x}Se$ shells as a function of the Zn/(Zn + Cd) molar ratio. (c) Raman spectra of the arrays of (i) ZnO/ZnSe, (ii) ZnO/$Zn_{0.7}Cd_{0.3}Se$, (iii) ZnO/$Zn_{0.33}Cd_{0.67}Se$, and (iv) ZnO/CdSe nanocables.

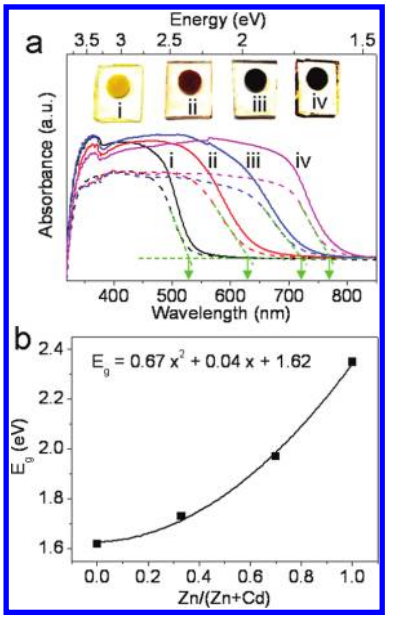

Figure 4. (a) UV−vis absorption spectra of the arrays of ZnO/$Zn_xCd_{1-x}Se$ ($0 \le x \le 1$) core/shell nanocables (solid lines) and the corresponding ternary $Zn_xCd_{1-x}Se$ shells prepared by removing the ZnO cores (dash lines). Curves of (i) ZnO/ZnSe nanocables, (ii) ZnO/$Zn_{0.7}Cd_{0.3}Se$ nanocables, (iii) ZnO/$Zn_{0.33}Cd_{0.67}Se$ nanocables, (iv) ZnO/CdSe nanocables. (b) A quadratic relationship of the band gaps of the ternary $Zn_xCd_{1-x}Se$ ($0 \le x \le 1$) nanotubes as a function of the Zn/(Zn + Cd) molar ratio. Inset of panel a: Photographs of the arrays of ZnO/$Zn_xCd_{1-x}Se$ nanocables.

10 nm thick. A single-crystalline core/polycrystalline shell structure is demonstrated by a high-resolution TEM image in Figure 2b. The fringe spacing of 0.53 nm in the single-crystalline core matches well to the interplanar spacing of the (0001) plane of hexagonal ZnO, while the fringe spacing of 0.29 nm in the polycrystalline shell matches well to the interplanar spacing of the {200} planes of cubic ZnSe. Figure 2c shows a nanocable with ternary alloyed shell of $Zn_{0.33}Cd_{0.67}Se$. A high-resolution TEM image of the ZnO/$Zn_{0.33}Cd_{0.67}Se$ nanocable is shown in Figure 2d. The fringe spacing of 0.34 nm in the polycrystalline shell is attributed to the interplanar spacing of the {111} planes of cubic $Zn_xCd_{1-x}Se$ alloy. The $Zn_xCd_{1-x}Se$ alloy is further characterized with electron energy loss spectroscopy (EELS). Figure S2a in the Supporting Information shows a TEM image of a ternary $Zn_{0.33}Cd_{0.67}Se$ shell prepared by dissolving the inner ZnO core from a ZnO/$Zn_{0.33}Cd_{0.67}Se$ nanocable in an acetic acid solution. Panels b−d of Figure S2 (Supporting Information) are, respectively, the corresponding Zn, Cd, and Se EELS elemental mappings, revealing that Zn, Cd, and Se are homogeneously distributed through the shell. TEM image (Figure 2e) and high-resolution TEM image (Figure 2f) of a ZnO/CdSe nanocable reveal the shell consists of CdSe nanoparticles with diameters of 10−15 nm. The fringe spacing of 0.35 nm of the nanoparticle matches well to the interplanar spacing of the {111} planes of the cubic CdSe.

Figure 3a shows XRD data of the arrays of the bare ZnO nanowires (labeled as ZnO) and the ZnO/$Zn_xCd_{1-x}Se$ nanocables (labeled as i−iv). The bottom curve for bare ZnO was measured from a sample of ZnO nanowire array grown on a FTO glass substrate. Diffraction peak positions of hexagonal ZnO and tetragonal SnO_2 from the FTO substrate are marked respectively with solid and dashed vertical lines. For curve i, the two diffraction peaks located at 27.5° and 45.5° can be respectively indexed to the (111) and the (220) planes of cubic ZnSe (JCPDF 37-1463), confirming again the formation of ZnSe shells. For curve iv, three peaks located at 25.5°, 42.1°, and 49.9° match well with the (111), (220), and (311) planes of cubic CdSe (JCPDF 19-0191), respectively, indicating the formation of CdSe shells. Curves ii and iii are from nanocables with ternary alloyed shells. It can be observed from the diffraction patterns of the ZnO/$Zn_xCd_{1-x}Se$ ($0 \le x \le 1$) nanocables that the diffraction peaks of (111) and (220) of the $Zn_xCd_{1-x}Se$ ($0 \le x \le 1$) phase show a systematic shift to lower 2θ degrees with increasing Cd content in the shells. It is due to the increased lattice spacing resulting from substitution of the smaller Zn atoms with the larger Cd atoms. As shown in Figure 3b, the lattice parameter a of the $Zn_xCd_{1-x}Se$ shells shows a linear relationship with the Zn content (x). This trend is consistent with the Vegard's law, which states that alloys show a linear relationship between the crystal lattice parameters and composition at constant temperature.[39−42] Formation of the ZnO/$Zn_xCd_{1-x}Se$ nanocable arrays with composition-tunable shells is further demonstrated by Raman studies as shown in Figure 3c. The Raman peaks of the first-order longitudinal optical phonon mode (LO) in the arrays of ZnO/$Zn_xCd_{1-x}Se$ nanocables show a systematic decrease from 250 cm^{-1} for ZnSe to 237 cm^{-1} for $Zn_{0.7}Cd_{0.3}Se$, 215 cm^{-1} for $Zn_{0.33}Cd_{0.67}Se$, and

dx.doi.org/10.1021/nl201934k |Nano Lett. 2011, 11, 4138–4143

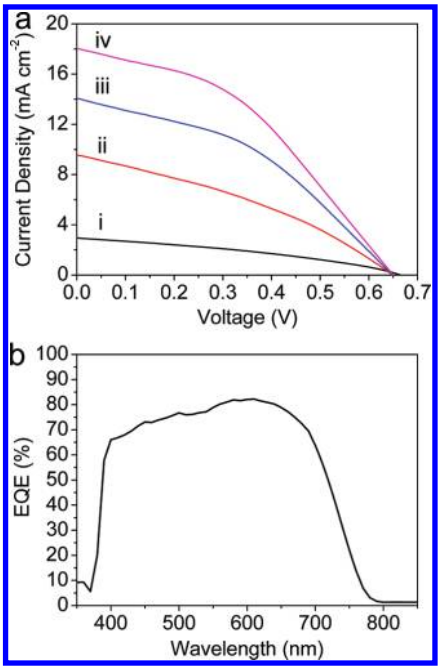

Figure 5. (a) Current density−voltage (J−V) characteristics of the PEC solar cells based on the arrays of ZnO/$Zn_xCd_{1-x}Se$ nanocables. Curves of (i) ZnO/ZnSe nanocables, (ii) ZnO/$Zn_{0.7}Cd_{0.3}Se$ nanocables, (iii) ZnO/$Zn_{0.33}Cd_{0.67}Se$ nanocables, and (iv) ZnO/CdSe nanocables. (b) EQE spectrum of the solar cell based on the ZnO/CdSe nanocable photoelectrode.

206 cm^{-1} for CdSe with decreasing Zn content. This continuous shift further confirms that the shell is a homogeneous ternary alloy of tunable compositions instead of a mixture of ZnSe and CdSe.[43−46]

Inset of Figure 4a shows photographs of the arrays of ZnO/$Zn_xCd_{1-x}Se$ nanocables. The sample color changed from yellow for the ZnO/ZnSe nanocables to bright red for the ZnO/$Zn_xCd_{1-x}Se$ nanocables and then to dark red for the ZnO/CdSe nanocables. Corresponding absorption spectra of the samples are shown in Figure 4a. All spectra of the ZnO/$Zn_xCd_{1-x}Se$ nanocables (solid lines) exhibit an absorption peak located at ∼363 nm, corresponding to the expected band gap (3.4 eV) absorption for bulk ZnO. To determine the absorption characteristics of the $Zn_xCd_{1-x}Se$ shells, ZnO cores of the cables were removed by etching in an acetic acid solution. Absorption spectra of the $Zn_xCd_{1-x}Se$ shells are shown as dashed lines in Figure 4a. Absorption edges of each sample of $Zn_xCd_{1-x}Se$ shells were estimated from the intersection points of two fitting lines,[14] the saturation and incline lines as shown in Figure 4a (marked in cyan).

It can be seen from Figure 4a that the optical absorption of the nanocables can be tuned to cover almost the entire visible spectrum. A systematic shift of the absorption edge of ZnO/$Zn_xCd_{1-x}Se$ nanocables (solid lines in Figure 4a) to longer wavelength (from 535 nm (2.32 eV), 643 nm (1.93 eV), and 725 nm (1.71 eV) to 776 nm (1.60 eV)) with decreasing Zn content in the ternary $Zn_xCd_{1-x}Se$ ($0 \le x \le 1$) shells was observed, demonstrating that band gap tuning stems from stoichiometry variation in the ternary alloy semiconductors. Furthermore, blue shifts of about 10 nm were observed upon removal of the ZnO core. The longer wavelength absorption in the cables can be explained by the type II electronic structures of the core/shell heterojunctions,[32−34] which enable an interface

Table 1. Photovoltaic Parameters Obtained from the J−V Curves Using the ZnO/$Zn_xCd_{1-x}Se$ Nanocable Arrays as Electrodes

nanocables	J_{SC} (mA cm^{-2})	V_{OC} (V)	FF	efficiency (%)
ZnO/ZnSe	2.94	0.67	0.34	0.68
ZnO/$Zn_{0.7}Cd_{0.3}Se$	9.54	0.65	0.34	2.12
ZnO/$Zn_{0.33}Cd_{0.67}Se$	14.07	0.65	0.40	3.65
ZnO/CdSe	18.05	0.65	0.40	4.74

transition coupling a hole state in the shell ($Zn_xCd_{1-x}Se$) with an electron state in the ZnO core. As the volume fraction of the interfacial region is small, the overall effects of such interfacial transition are thus not obvious.

While the lattice parameter of ternary alloys ($A_xB_{1-x}C$) changes linearly with composition, band gaps often vary nonlinearly. To a first approximation, the variation is quadratic.[10,45−48]

$$E_g(A_xB_{1-x}C) = xE_g(AC) + (1-x)E_g(BC) - bx(1-x)$$

where b is a bowing parameter, describing the extent of nonlinearity.

In our case, the variation of the band gaps of the $Zn_xCd_{1-x}Se$ shell with Zn content (x) is shown in Figure 4b and can be fitted with a quadratic function of $E_g = 0.67x^2 + 0.04x + 1.62$ ($0 \le x \le 1$) with a bowing parameter of 0.67 eV. According to a theoretical model developed by Zunger and co-workers, the observed band gap bowing may arise from three structural and electronic factors: (i) the volume deformation resulted from the changing lattice constant which alters the band structure; (ii) the electronegativity difference of the atoms in the alloy deforming the electron distribution; and (iii) the internal structural relaxation of the anion−cation bond lengths and angles to accommodate the differently sized constituents.[49,50]

Using the various ZnO/$Zn_xCd_{1-x}Se$ nanocable arrays as the photoanodes, we fabricated photoelectrochemical (PEC) solar cells to evaluate their photovoltaic (PV) performances. PV characterization for all cells, with an active cell area of 0.28 cm^2, was measured under AM 1.5G simulated sunlight with an intensity of 100 mW cm^{-2}. Figure 5a shows the current density−voltage (J−V) characteristics of the cells. The measurement results from various nanocables are summarized in Table 1. The cell based on an array of ZnO/ZnSe nanocables (curve i) gives a short-circuit current density (J_{SC}) of 2.94 mA cm^{-2}, an open-circuit voltage (V_{OC}) of 0.67 V, and a fill factor (FF) of 0.34, yielding a power conversion efficiency (η) of 0.68%. With increasing Cd content in the shells, both the J_{SC} and η drastically increase to 9.54 mA cm^{-2} and 2.12% for ZnO/$Zn_{0.7}Cd_{0.3}Se$ nanocables (curve ii), to 14.07 mA cm^{-2} and 3.65% for ZnO/$Zn_{0.33}Cd_{0.67}Se$ nanocables (curve iii), and 18.05 mA cm^{-2} and 4.74% for ZnO/CdSe nanocables (curve iv) while their V_{OC} remain at about 0.65 V. The increasing J_{SC} is mainly due to the expanded absorption spectrum coverage of the ZnO/$Zn_xCd_{1-x}Se$ nanocables with more Cd. The increase in FF is probably due to the smaller serial resistances in the devices with high Cd content. Details are discussed in Table S1 of Supporting Information. The external quantum efficiency (EQE) of the solar cell based on the ZnO/CdSe nanocables is shown in Figure 5b. A broad >65% EQE plateau in the spectrum from 400 to 700 nm and a maximum 82% EQE value at 610 nm can be observed. Integration of the EQE spectrum shows that the J_{SC} is about 17.5 mA cm^{-2}, which is consistent with the data from the J−V curve.

dx.doi.org/10.1021/nl201934k |*Nano Lett.* 2011, 11, 4138–4143

The high performance may be attributed to the ZnO/CdSe core/shell nanocables possessing uniform coverage and effective loading of CdSe without any organic linker species used in the preparation, which is usually unavailable for QDSSC due to low loading density of quantum dots on the surface of ZnO nanowires. The shells of the nanocables may serve as a passivation layer that protects the ZnO from etching by the electrolyte and also inhibits recombination of percolated electrons in the ZnO nanowires with the electrolyte. On the other hand, if the Cd^{2+} ion exchange reaction was carried out at 160 °C, the CdSe nanoparticles with sizes of 15−20 nm cannot form a continuous and uniform shell on the ZnO nanowires (Figure S3a of Supporting Information). Solar cell fabricated with this sample showed poorer photovoltaic performance (panels b and c of Figure S3, Supporting Information). This result further reveals the importance of uniform shells in nanocables for photovoltaic applications. Furthermore, The Cu_2S electrode and polysulfide electrode contribute to provide high photocurrent density.[51,52]

In summary, a series of arrays of ZnO/$Zn_xCd_{1-x}Se$ ($0 \le x \le 1$) nanocables with tunable shell compositions have been prepared by using a simple ion-exchange method. While the lattice parameter of the ternary alloyed $Zn_xCd_{1-x}Se$ shells shows a linear relationship with the Zn content (x), the band gap varies quadratically with the Zn content (x). Continuous tuning of optical absorption covering nearly the entire visible light region has been achieved by controlling their shell composition without changing the nanocable size. The ability for the continuous and controllable tuning of composition and band gap is promising to allow these nanocables to fulfill their full potential in different specific applications. The core/shell configuration, the type II band alignment, the shell passivation, and the favorable absorption properties of CdSe contribute to high photovoltaic performance for the ZnO/CdSe nanocables with a maximum power conversion efficiency up to 4.74%. The flexibility of tailoring various materials via the simple ions-exchange approach makes it a very promising synthetic method for preparation of ZnO-based heterostructures with custom-designed properties for different applications.

■ ASSOCIATED CONTENT

Supporting Information. Experimental details, EDX spectra of the $Zn_xCd_{1-x}Se$ ($0 \le x \le 1$) shells, EELS mapping of the $Zn_{0.33}Cd_{0.67}Se$ shell, EQE spectrum, and $J-V$ characteristic of the solar cell based on ZnO/CdSe photoanode prepared at 160 °C. This material is available free of charge via the Internet at http://pubs.acs.org.

■ AUTHOR INFORMATION

Corresponding Author
*E-mail: apcslee@cityu.edu.hk (C.S. Lee).

■ ACKNOWLEDGMENT

This project has been financially supported by Research Grants Council of HKSAR (No. CityU 101910). The authors thank Mr. T. F. Hung for TEM and EELS characterization.

■ REFERENCES

(1) Peng, X. G. *Acc. Chem. Res.* **2010**, *43*, 1387–1395.
(2) Regulacio, M. D.; Han, M.-Y. *Acc. Chem. Res.* **2010**, *43*, 621–630.
(3) Smith, A. M.; Nie, S. M. *Acc. Chem. Res.* **2010**, *43*, 190–200.
(4) Ma, D. D. D.; Lee, C. S.; Au, F. C. K.; Tong, S. Y.; Lee, S. T. *Science* **2003**, *299*, 1874–1877.
(5) Sun, J.; Buhro, W. E.; Wang, L.-W.; Schrier, J. *Nano Lett.* **2008**, *8*, 2913–2919.
(6) Barnard, A. S. *Cryst. Growth Des.* **2009**, *9*, 4860–4863.
(7) Zhong, X.; Feng, Y.; Knoll, W.; Han, M. *J. Am. Chem. Soc.* **2003**, *125*, 13559–13563.
(8) Zhong, X.; Han, M.; Dong, Z.; White, T. J.; Knoll, W. *J. Am. Chem. Soc.* **2003**, *125*, 8589–8594.
(9) Bailey, R. E.; Nie, S. M. *J. Am. Chem. Soc.* **2003**, *125*, 7100–7106.
(10) Swafford, L. A.; Weigand, L. A.; Bowers, M. J., II; McBride, J. R.; Rapaport, J. L.; Watt, T. L.; Dixit, S. K.; Feldman, L. C.; Rosenthal, S. J. *J. Am. Chem. Soc.* **2006**, *128*, 12299–12306.
(11) Lo, S. S.; Mirkovic, T.; Chuang, C.-H.; Burda, C.; Scholes, G. D. *Adv. Mater.* **2011**, *23*, 180–197.
(12) Ivanov, S. A.; Piryatinski, A.; Nanda, J.; Tretiak, S.; Zavadil, K. R.; Wallace, W. O.; Werder, D.; Klimov, V. I. *J. Am. Chem. Soc.* **2007**, *129*, 11708–11719.
(13) Pan, A. L.; Yao, L.; Qin, Y.; Yang, Y.; Kim, D. S.; Yu, R.; Zou, B.; Werner, P.; Zacharias, M.; Gösele, U. *Nano Lett.* **2008**, *8*, 3413–3417.
(14) Sung, T. K.; Kang, J. H.; Jang, D. M.; Myung, Y.; Jung, G. B.; Kim, H. S.; Jung, C. S.; Cho, Y. J.; Park, J.; Lee, C.-L. *J. Mater. Chem.* **2011**, *21*, 4553–4561.
(15) Liu, H.; She, G.; Ling, S.; Mu, L.; Shi, W. *J. Appl. Phys.* **2011**, *109*, 044305.
(16) Sun, W.-T.; Yu, Y.; Pan, H.-Y.; Gao, X.-F.; Chen, Q.; Peng, L.-M. *J. Am. Chem. Soc.* **2008**, *130*, 1124–1125.
(17) Wang, H.; Bai, Y.; Zhang, H.; Zhang, Z.; Li, J.; Guo, L. *J. Phys. Chem. C* **2010**, *114*, 16451–16455.
(18) Lee, W.; Min, S. K.; Dhas, V.; Ogale, S. B.; Han, S.-H. *Electrochem. Commun.* **2009**, *11*, 103–106.
(19) Leschkies, K. S.; Divakar, R.; Basu, J.; Enache-Pommer, E.; Boercker, J. E.; Carter, C. B.; Kortshagen, U. R.; Norris, D. J.; Aydil, E. S. *Nano Lett.* **2007**, *7*, 1793–1798.
(20) Wang, G.; Yang, X.; Qian, F.; Zhang, J. Z.; Li, Y. *Nano Lett.* **2010**, *10*, 1088–1092.
(21) Hensel, J.; Wang, G.; Li, Y.; Zhang, J. Z. *Nano Lett.* **2010**, *10*, 478–483.
(22) López-Luke, T.; Wolcott, A.; Xu, L.-p.; Chen, S.; Wen, Z.; Li, J.; De La Rosa, E.; Zhang, J. Z. *J. Phys. Chem. C* **2008**, *112*, 1282–1292.
(23) Aga, R. S.; Jowhar, D.; Ueda, A.; Pan, Z.; Collins, W. E.; Mu, R.; Singer, K. D.; Shen, J. *Appl. Phys. Lett.* **2007**, *91*, 232108.
(24) Cao, X.; Chen, P.; Guo, Y. *J. Phys. Chem. C* **2008**, *112*, 20560–20566.
(25) Kuo, K.-T.; Liu, D.-M.; Chen, S.-Y.; Lin, C.-C. *J. Mater. Chem.* **2009**, *19*, 6780–6788.
(26) Yuhas, B. D.; Yang, P. D. *J. Am. Chem. Soc.* **2009**, *131*, 3756–3761.
(27) Guijarro, N.; Lana-Villarreal, T.; Mora-Seró, I.; Bisquert, J.; Gómez, R. *J. Phys. Chem. C* **2009**, *113*, 4208–4214.
(28) Liu, L.; Hensel, J.; Fitzmorris, R. C.; Li, Y.; Zhang, J. Z. *J. Phys. Chem. Lett.* **2010**, *1*, 155–160.
(29) Hodes, G. *J. Phys. Chem. C* **2008**, *112*, 17778–17787.
(30) Kayes, B. M.; Atwater, H. A.; Lewis, N. S. *J. Appl. Phys.* **2005**, *97*, 114302.
(31) Tian, B.; Zheng, X.; Kempa, T. J.; Fang, Y.; Yu, N.; Yu, G.; Huang, J.; Lieber, C. M. *Nature* **2007**, *449*, 885–890.
(32) Wang, K.; Chen, J. J.; Zhou, W. L.; Zhang, Y.; Yan, Y. F.; Pern, J.; Mascarenhas, A. *Adv. Mater.* **2008**, *20*, 3248–3253.
(33) Schrier, J.; Demchenko, D. O.; Wang, L.-W. *Nano Lett.* **2007**, *7*, 2377–2382.
(34) Kim, S.; Fisher, B.; Eisler, H. J.; Bawendi, M. *J. Am. Chem. Soc.* **2003**, *125*, 11466–11467.
(35) Tsakalakos, L. *Mater. Sci. Eng. R* **2008**, *62*, 175–189.
(36) Wang, X.; Zhu, H.; Xu, Y.; Wang, H.; Tao, Y.; Hark, S.; Xiao, X.; Li, Q. *ACS Nano* **2010**, *4*, 3302–3308.
(37) Seol, M.; Kim, H.; Tak, Y.; Yong, K. *Chem.Commun.* **2010**, *46*, 5521–5523.

(38) Xu, J.; Luan, C.-Y.; Tang, Y.-B.; Chen, X.; Zapien, J. A.; Zhang, W.-J.; Kwong, H.-L.; Meng, X.-M.; Lee, S.-T.; Lee, C.-S. *ACS Nano* **2010**, *4*, 6064–6070.
(39) Vegard, L. *Z. Phys.* **1921**, *5*, 17–26.
(40) Denton, A. R.; Ashcroft, N. W. *Phys. Rev. A* **1991**, *43*, 3161–3164.
(41) Furdyna, J. K. *J. Appl. Phys.* **1988**, *64*, R29.
(42) Xu, J.; Tang, Y.-B.; Chen, X.; Luan, C.-Y.; Zhang, W.-F.; Zapien, J. A.; Zhang, W.-J.; Kwong, H.-L.; Meng, X.-M.; Lee, S.-T.; Lee, C.-S. *Adv. Funct. Mater.* **2010**, *20*, 4190–4195.
(43) Tu, A.; Persans, P. D. *Appl. Phys. Lett.* **1991**, *58*, 1506–1508.
(44) Azhniuk, Y. M.; Hutych, Y. I.; Lopushansky, V. V.; Prots, L. A.; Gomonnai, A. V.; Zahn, D. R. T. *Phys. Status Solidi C* **2009**, *6*, 2064–2067.
(45) Venugopal, R.; Lin, P.-I.; Chen, Y.-T. *J. Phys. Chem. B* **2006**, *110*, 11691–11696.
(46) Yoon, Y.-J.; Park, K.-S.; Heo, J.-H.; Park, J.-G.; Nahm, S.; Choi, K. J. *J. Mater. Chem.* **2010**, *20*, 2386–2390.
(47) Liou, B.-T.; Yen, S.-H.; Kuo, Y.-K. *Appl. Phys. A: Mater. Sci. Process.* **2005**, *81*, 651–655.
(48) Wang, M.; Fei, G. T.; Zhang, Y. G.; Kong, M. G.; Zhang, L. D. *Adv. Mater.* **2007**, *19*, 4491–4494.
(49) Bernard, J. E.; Zunger, A. *Phys. Rev. B* **1987**, *36*, 3199–3226.
(50) Wei, S.-H.; Zhang, S. B.; Zunger, A. *J. Appl. Phys.* **2000**, *87*, 1304–1311.
(51) González-Pedro, V.; Xu, X.; Mora-Seró, I.; Bisquert, J. *ACS Nano* **2010**, *4*, 5783–5790.
(52) Yang, Z.; Chen, C.-Y.; Liu, C.-W.; Chang, H.-T. *Chem.Commun.* **2010**, *46*, 5485–5487.